

Time evolution of spread complexity in quenched Lipkin-Meshkov-Glick model

Mir Afrasiar, Jaydeep Kumar Basak, Bidyut Dey, Kunal Pal, Kuntal Pal¹

Department of Physics, Indian Institute of Technology - Kanpur, Kanpur 208016, India

E-mail: afrasiar@iitk.ac.in, jaydeep@iitk.ac.in, bidyutd@iitk.ac.in,
kunalpal@iitk.ac.in, kuntal@iitk.ac.in

ABSTRACT: We use the spread complexity of a time evolved state after a sudden quantum quench in the Lipkin-Meshkov-Glick (LMG) model prepared in the ground state as a probe of equilibrium signatures of quantum phase transition when the system is quenched towards the critical point from either of the phases of the system. Utilizing the increment in the effective number of elements of the Krylov basis those contribute to the spread complexity more than a preassigned cut off, we show how the two phases of the LMG model can be distinguished. We also explore the time evolution of spread entropy after both non-critical and critical quenches and show that the sum contributing to the spread entropy converges slowly in the symmetric phase of the LMG model compared to that of the broken phase. For a critical quench the spread entropy diverges logarithmically at late times.

arXiv:2208.10520v1 [hep-th] 22 Aug 2022

¹Corresponding author

Contents

1	Introduction	1
2	Spread complexity over Krylov basis	4
3	Spread complexity in instantaneous quantum quenches of the LMG model	6
3.1	Thermodynamic limit of the LMG model	7
3.2	Time evolved state after a sudden quantum quench	8
3.3	The Lanczos coefficients and the spread complexity	10
3.4	Complexity evolution after a critical quench and dependence on the initial state	17
4	Time Evolution of spread entropy	18
4.1	Post-quench evolution of spread entropy	19
4.2	Evolution of spread entropy in the critical quench	21
5	Conclusions	22
A	Spread complexity in quantum quench of the SSH model	24

1 Introduction

Understanding the notion of complexity in quantum systems and field theory has gained a lot of attention recently. One of the reasons behind this surge of interest is the notion that this quantity can be used as a probe of black hole interiors, and this has been conjectured to be given in terms of either the volume or the gravitational action [1]. From the viewpoint of the gauge-gravity duality, the important question to ask is, what observable would be dual to the complexity of a black hole in terms of a well defined quantity on the field theory side. On the other hand, the notion of circuit complexity (CC) in quantum systems that is extensively used in computer science is defined as the difficulty of preparing a ‘target state’ starting from a particular ‘reference state’ using a given set of unitary operators as basic building blocks. Among the most used formulations of the above statement, two of the popular notions are the ‘Nielsen complexity’ and the ‘Fubini-Study complexity’. Introduced in [2], the Nielsen complexity (NC) measures the minimum of a particular cost functional to implement a given task, which can be expressed as the geodesic distance in a Riemannian manifold constructed from the unitary operator connecting the reference and the target state. Originally defined in terms of the discrete gate sets, a notion of NC for field theory was given in [3] which was further elaborated in the works of [4, 5]. A slightly different notion of complexity is to measure the geodesics distance on the Riemannian parameter

manifold of a Hamiltonian, which is induced with the Fubini-Study metric - subsequently called as the Fubini-study complexity (FSC) [6]. Related to these two popular ways of calculating the complexity, there are also related avenues that have been explored recently to quantify circuit complexity. For example, several works have appeared related to the bi-invariant complexity (which is particularly important for studying complexity in QFTs) [7], complexity from covariance matrix [8, 9], complexity from the information geometry [10], path integral approach to circuit optimization [11], possible extensions to conformal field theories [12, 13] (see the recent review [14] and references therein). In this work we explore a relatively new notion of complexity, namely the spread complexity of a time evolved target state, when the parameters of a quantum many-body system showing quantum phase transition is suddenly quenched to a new set of values.

The above mentioned measures of complexity have also found important applications in the context of quantum many body physics. The three broad sub-areas where the CC have been used recently are (1) studying quantum phase transitions, (2) probing non-equilibrium dynamics, typically following a quantum quench and (3) and as an indicator of quantum chaos. Starting from the work of [15], which shows nonanalytical behaviors of the NC at the critical points for topological phase transitions in the Kitaev chain, there are quite a few works in this direction to study zero temperature quantum phase transition (QPT) [16]. The motivation behind these kinds of studies is to notice that an observable will fail to be analytic with a continuous change of the parameters characterizing the Hamiltonian. For example, the authors of [17] used NC as a probe of topological phase transition in one and two dimensions.

The work of [18] elaborates the use of both NC and FSC to detect ground state QPT in transverse field Ising models. Evolution of NC for quench dynamics in transverse field Ising model was studied in [19] and for periodic driving in [20].

The Behaviors of CC were explored for the Bose-Hubbard model in [21, 22] and for the infinite range Lipkin-Meshkov-Glick (LMG) model in [23]. On the other hand, the time evolution of CC under a quantum quench and its comparison with entanglement measures of a system can reveal a great deal of information about the underlying dynamics, depending on the integrability property of the Hamiltonian. Works in these directions include CC evolution under smooth mass quench in free field theory [24], scaling of complexity in different quench regions [25], distinctions between different proposals for complexity following a quench [26] and multiple quenches [27, 28]. Time evolution of CC involving a classically chaotic Hamiltonian can be used as an effective probe for still elusive quantum signatures of chaos as demonstrated in [29, 30].

One of the still ambiguous features of Nielsen type complexities is the choice of the so called ‘cost functional’ associated with a particular path in the unitary manifold. In the original formulation of Nielsen in the context of quantum computation, the choice of the gate sets and their associated paths are in one’s hand, and the cost selection is somewhat natural. However, this statement is not appropriate for the case of real life quantum systems and field theories [31, 32]. Consequently, there is still scope for refining the exact nature of quantum state complexity, which is dual to holographic complexity. In view of the above discussions, a new measure of complexity named the ‘spread complexity’ for quantum states

has gained significant attention. Introduced originally in the context of operator growth in quantum systems, the ‘Krylov complexity’ (KC) measures how an initial simple operator becomes complex under the evolution of a chaotic Hamiltonian [33]. The key aspect of calculating the KC includes finding the Krylov basis, an orthonormal basis in the operator Hilbert space. The canonical way for constructing the same is to implement the so called ‘Lanczos algorithm’ [34]. Roughly the Lanczos algorithm is an iterative procedure that gives two sets of constants a_n and b_n as output with the auto-correlation function, the inner overlap of a time evolved state at an arbitrary time with the state at the initial time, provided as an input. It was conjectured that the linear growth of the quantity b_n implies a chaotic nature of the evolution [33]. Various aspects of this conjecture and possible way of finding the Lanczos coefficients by means of analytical and numerical tools were elaborated in [35–55]. In a slightly different context, the approach to defining the Krylov subspace and corresponding complexity directly for the unitary evolution of an initial state under a Hamiltonian was introduced in [56]. It was shown in this reference that the spread of a wave function over all choices of the basis on the Hilbert space is minimized when the orthonormal basis is the Krylov basis constructed from the reference state as the starting point. In this case, the complete sets of the Lanczos coefficients can be obtained from the ‘survival amplitude’, which is the overlap between the initial reference state and the unitary evolved target state. This notion of spread complexity was explored further in [57] to distinguish different topological phases of the Su-Schrieffer-Heeger (SSH) model and in Kitaev chain [58]. It was concluded that the spread complexity shows markedly different behavior in two phases, in contrast to that of the NC. The authors of [59] used spread complexity of time evolved states to probe weak ergodicity-breaking in the scar states - the states that weakly violate the eigenstate thermalization hypothesis.

A generic quantum many body system can show signatures of equilibrium quantum phase transition even when the system is kicked out of equilibrium by employing a sudden change in the parameters of the Hamiltonian. Various information theoretic measures like time dependent fidelity, average work, and irreversible work have been used to locate static critical points. In this article, our interest is to study the equilibrium signatures of quantum phase transition when a many body system having infinite range interaction is driven towards its quantum critical point, by using the spread complexity of the time evolved state as a possible probe. To this end we use the LMG model as a prototype quantum system having infinite range interaction between its constituting particles. Though, due to the long-range nature of the interaction, it cannot be mapped to free fermion models, in the thermodynamic limit the phases of this model can be worked out, and have been studied extensively in the literature [60, 61]. Besides these works on the static properties of the LMG model, the time-dependent fidelity in a quench scenario was studied [62], the Nielsen and Fubini-Study complexity in [23, 63] - where all these quantities have been shown to have some particular behavior as the system moves towards the critical point.

In this paper, we first construct the Krylov basis, by implementing the Lanczos algorithm starting from the pre-quenched LMG model ground state in either of the two characteristic phases of the system. We then obtain the Lanczos coefficients numerically [34], and also provide a compact form of these coefficients, which are then used to generate

an analytical expression for the time evolution of the spread complexity of the time evolved state after a sudden quench of the parameters of the LMG model. The spread complexity shows complete revivals while the target state is away from the critical point, and the magnitudes of these oscillations grow as the system is moved towards the critical point. To systematically characterize this growth, we define a new quantity N_{eff} , which we call the effective number of elements of the Krylov basis which contribute to the growth of the spread complexity, up to a predefined cutoff, and it is shown that this quantity grows as the critical point is approached. Furthermore, it is shown that the growth of N_{eff} is different on the two sides of the critical point, thereby providing a way to distinguish between them in a quench process. When the quench is a critical quench we show that the spread complexity grows quadratically with time, and hence, diverges late times.

Furthermore we also study the analogue of K-entropy, defined as spread entropy, in the context of Hamiltonian evolution. The spread entropy shows oscillatory behavior for noncritical quench, while for the critical quench, it shows logarithmic divergence at late times.

The paper is structured as follows. In sec. (2) we review the basic structure of Krylov complexity and the Lanczos algorithm. In sec. (3) we study the time evolution of spread complexity for the quenched LMG model. We start with a concise review of the thermodynamic limit of the LMG model in sec. (3.1). Subsequently we analyze the time evolution of the LMG ground state under the quenched Hamiltonian and compute the Lanczos coefficients and the spread complexity in sections (3.2) and (3.3) respectively. Then we conclude the study of spread complexity for LMG model by analyzing its behavior for both non-critical and critical quenches in sec. (3.4). In sec. (4) we study the spread entropy, where the time evolution is studied for the critical and non critical quenches. Finally we summarize our findings in sec. (5). The paper also contains an appendix where we briefly analyse the spread complexity in the SSH model when the initial state is not the ground state of SSH Hamiltonian.

2 Spread complexity over Krylov basis

The circuit complexity to prepare a quantum target state $|\psi_T\rangle$ starting from a reference state $|\psi_R\rangle$ where the latter is related to the former by a unitary transformation, is defined as the minimum number of fundamental gates required in the process. There exist various approaches in the literature for calculating the complexity of a given quantum state transformation. One of the most popular approaches is Nielsen’s geometric formulation, where the circuit complexity is given by the minimum value of a particular cost functional assigned to each path on a Riemannian manifold obtained from the unitary transformation connecting the reference and the target states. This procedure essentially reduces to calculating the geodesic distance between two points on the unitary manifold representing the target and the reference states, respectively.

On the other hand, a somewhat more direct approach which is motivated by the notion of Krylov complexity of operator growth in quantum chaotic systems is the recently introduced notion of ‘spread complexity’ over the basis in the Hilbert space of a particular

quantum system. To elaborate, let us consider the evolution of a state under a ‘protocol Hamiltonian’ H , as

$$|\psi(s)\rangle = e^{-iHs} |\psi(s=0)\rangle . \quad (2.1)$$

Here s is an arbitrary parameter characterizing the reference state ($s=0$) and the target state ($s=1$). For time evolutions generated by a system’s time-independent quantum mechanical Hamiltonian, this parameter is the time. The basic goal of defining the spread complexity is to precisely quantify how the reference state $|\psi_R\rangle$ spreads over the Hilbert space. To this end, one first defines a measure of this spreading i.e., a cost function as

$$\mathcal{C}_B(s) = \sum_n n |\langle \psi(s) | B_n \rangle|^2 , \quad (2.2)$$

with respect to some particular complete orthonormal basis $B = \{|B_n\rangle, n = 0, 1, 2, \dots\}$. Here, the cost function is defined in such a way that it will increase if a given wavefunction spreads deeper in the basis B . The minimization of this cost function over all the possible choices of the bases defines the spread complexity.

Among all the choices of the bases B , a particular basis, known as the Krylov basis, plays the most significant role in defining the spread complexity. The Krylov basis ($|K_n\rangle, n = 0, 1, 2, \dots$), as an orthonormal set of base kets, can be obtained using the Gram-Schmidt orthogonalisation procedure on the basis kets of the expansion of eq. (2.1). This particular basis is convenient for studying the spread of the initial state over the full Hilbert space.

The key idea behind the construction of the Krylov basis is to write the Hamiltonian in the tri-diagonal basis in the Lanczos algorithm. In this procedure a new basis is defined in terms of the old basis as follows,

$$|K_{n+1}\rangle = \frac{1}{b_{n+1}} \left[(H - a_n) |K_n\rangle - b_n |K_{n-1}\rangle \right] . \quad (2.3)$$

Here $|K_0\rangle = |\psi(0)\rangle$ implies that the algorithm starts with the reference state. The computation of the coefficients a_n, b_n , known as the Lanczos coefficients, plays a pivotal role in implementing the Lanczos algorithm. This information about the Lanczos coefficients is also encoded in the so called ‘return-amplitude’, which is defined as the overlap between the state at any particular value of the circuit parameter s and the initial state, i.e

$$\mathcal{S}(s) = \langle \psi(s) | \psi(0) \rangle . \quad (2.4)$$

The return amplitude is the analogue of the auto-correlation function in the Liouvillian recursion. The expansion of the target state in terms of the Krylov basis is given by

$$|\psi(s)\rangle = \sum_n \phi_n(s) |K_n\rangle , \quad (2.5)$$

where, the expansion coefficients $\phi_n(s)$ satisfy the discrete Schrödinger equation

$$i\partial_s \phi_n(s) = a_n \phi_n(s) + b_n \phi_{n-1}(s) + b_{n+1} \phi_{n+1}(s) . \quad (2.6)$$

The fact that the Krylov basis defined above minimizes the cost function in eq. (2.2) has been proved recently in [56]. In the Krylov basis, the expression of the spread complexity becomes particularly simple and given by

$$\mathcal{C}(s) = \sum_n n |\phi_n(s)|^2 . \quad (2.7)$$

The next two important steps in the procedure of evaluating the spread complexity consists of determining the Lanczos coefficients from the return amplitude, and finding the $\phi_n(s)$ from the eq. (2.6). For calculating the Lanczos coefficients from the return amplitude, we first need to extract the even and odd moments from the expansion as,

$$\mathcal{S}(s) = \sum_n M_n \frac{s^n}{n!} . \quad (2.8)$$

From the known full sets of moments, we can extract the sets a_n and b_n using the standard recursion methods available in the literature [34]. Once we know the a_n s and b_n s, we can solve the discrete Schrödinger equation (2.6), for each value of n and obtain ϕ_n with the initial condition $\phi_n(0) = \delta_{n,0}$. We use this procedure to study the time evolution of the spread complexity in sudden quenches of some known quantum systems.

3 Spread complexity in instantaneous quantum quenches of the LMG model

In this section, we study the spread complexity in quantum quenches of some well known models of many-body physics. The time evolution of the spread complexity can be computed following a few simple steps. For many-body systems we consider a quench protocol where the system parameters are changed instantaneously to a new set of values. We assume that the pre-quenched system is prepared in the lowest state of the Krylov basis, i.e. $|K_0\rangle = |\psi(t=0)\rangle = |\psi_i\rangle$, which is not necessarily the ground state of the system Hamiltonian H_i . At $t=0$, we perform the sudden quench changing the system Hamiltonian H_f , which subsequently drives the time evolution. The state at any arbitrary time t after the quench can be expressed as

$$|\Psi_f(t)\rangle = e^{-iH_f t} |\psi(t=0)\rangle = e^{-iH_f t} |K_0\rangle . \quad (3.1)$$

Comparing the above equation with eq. (2.1), one can assume that the real time t plays the role of circuit time s explained in section 2. Hence the return amplitude, containing all the information about the Lanczos coefficients, is expressed by the following inner product

$$\mathcal{S}(t) = \langle \Psi_f(t) | \psi(t=0) \rangle = \langle \psi(t=0) | e^{iH_f t} | \psi(t=0) \rangle . \quad (3.2)$$

Utilizing eq. (3.2), we compute all the Lanczos coefficients which are used to find out the $\phi_n(t)$ s by solving the discrete Schrödinger equation (2.6). Following eq. (2.7), we determine the spread complexity as a function of time using the Lanczos coefficients mentioned before.

In this article, we mainly focus on the Lipkin-Meshkov-Glick (LMG) model [64] of nuclear physics, which is one of the most studied example of many-body system involving

infinite range interactions. This model also shows a quantum phase transition at critical values of the parameters involved. Considering appropriate Bogoliubov transformations, the LMG model can be diagonalized in the thermodynamic limit. These mathematical tricks make the computations of the spread complexity simple, as we show in sequel.

In appendix A we briefly consider the time evolution of the spread complexity after a quantum quench in the Su-Schrieffer-Heeger (SSH) model to illustrate the difference between the results in the SSH and the LMG model.

3.1 Thermodynamic limit of the LMG model

The LMG model describes N spin 1/2 self interacting particles acted upon by an external field. The Hamiltonian of this model can be written in terms of components J_α (with $\alpha = \{x, y, z\}$) of a collective spin operator J as

$$\mathcal{H} = -\frac{2}{N} (J_x^2 + \gamma J_y^2) - 2hJ_z, \quad (3.3)$$

where we have neglected an irrelevant constant energy shift [65]. In the above equation, h is an externally applied magnetic field, which for convenience we assume to be along the z direction. The anisotropy of the spin-spin interaction is characterized by the constant γ which varies in the range $0 \leq \gamma \leq 1$.

The ground state of this model exhibits a second order QPT in the thermodynamic limit $N \rightarrow \infty$ of this Hamiltonian, when the value of the external field approaches a critical value $h_c \rightarrow 1$ [60, 61]. In this paper, all the results are obtained considering the thermodynamic limit of the LMG model. Furthermore, assuming that the external field can only take positive values $h > 0$, we need to consider two different phases. The first phase, characterized by the magnetic field in the range $0 \leq h \leq 1$, is called the symmetry broken phase (BP) [65]. On the other hand, for $h > 1$, the system is in the symmetric phase (SP). In both phases, the leading order terms contributing to the Hamiltonian in the thermodynamic limit can be obtained in terms of the bosonic creation and annihilation operators using the Holstein-Primakoff representation of the spin components J_α . This Hamiltonian can now be diagonalized using a Bogoliubov transformation. For brevity, we leave out the standard details of this procedure ¹ and provide only the final form of the Hamiltonian in terms of the final set of creation and annihilation operators.

In the symmetry broken phase, the final form of the Hamiltonian can be written in terms of the bosonic operators $\alpha_1, \alpha_1^\dagger$ as

$$\mathcal{H}_{BP} = 2\sqrt{(1-h^2)(1-\gamma)} \left(\alpha_1^\dagger \alpha_1 + \frac{1}{2} \right). \quad (3.4)$$

Whereas in the symmetric phase, we define the new set of bosonic operators $\alpha_2, \alpha_2^\dagger$ utilizing the Bogoliubov transformation and the final form of the Hamiltonian after the diagonalization is given by

$$\mathcal{H}_{SP} = 2\sqrt{(h-1)(h-\gamma)} \left(\alpha_2^\dagger \alpha_2 + \frac{1}{2} \right). \quad (3.5)$$

¹see [65] for details of this diagonalization procedure.

Thus, in both phases, the final form of the Hamiltonian is that of a simple harmonic oscillator written in terms of the corresponding creation and annihilation operator. We also note that the Bogoliubov transformation is different in the two phases of the system. As the system approaches the QPT, the frequency of the corresponding oscillator from either phase goes to zero.

3.2 Time evolved state after a sudden quantum quench

The quench protocol we consider is the following, where the LMG model is assumed to be in the ground state with the values of the parameter h_i and γ_i . The system can either be in the BP or the SP, depending on the initial magnetic field h_i . At $t = 0$, we suddenly change the magnetic field to a new value h_f so that the new parameter h_f still characterizes the same phase as the initial one. Thus the phase of the LMG model before and after the quench is assumed to remain the same. We can also suddenly change the anisotropy parameter γ_i to a new value γ_f . However, in the numerical calculations below, we mostly keep it to be a constant.

To find out the time evolved state after the quench in eq. (3.1), we need to write down the Hamiltonian \mathcal{H}_f after the quench in terms of the operators α_{ji} and α_{ji}^\dagger ($j = 1, 2$) before the quench. This can be accomplished by realizing that the bosonic operators before and after the quench are related by a Bogoliubov transformation [26]

$$\begin{pmatrix} \alpha_{jf} \\ \alpha_{jf}^\dagger \end{pmatrix} = \begin{pmatrix} \mathcal{U}_j & \mathcal{V}_j \\ \mathcal{V}_j & \mathcal{U}_j \end{pmatrix} \begin{pmatrix} \alpha_{ji} \\ \alpha_{ji}^\dagger \end{pmatrix}, \quad (3.6)$$

where the Bogoliubov coefficients are $\mathcal{U}_j = \frac{\omega_{jf} + \omega_{ji}}{2\sqrt{\omega_{ji}\omega_{jf}}}$, $\mathcal{V}_j = \frac{\omega_{jf} - \omega_{ji}}{2\sqrt{\omega_{ji}\omega_{jf}}}$. Here the subscript j indicates which of the two phases of the LMG model we are considering. In terms of the operators before the quench, the post-quench Hamiltonian can then be written as

$$\mathcal{H}_f = 2\omega_{jf} \left[\mathcal{U}_j \mathcal{V}_j K^+ + (\mathcal{U}_j^2 + \mathcal{V}_j^2) K^0 + \mathcal{U}_j \mathcal{V}_j K^- \right]. \quad (3.7)$$

Here the operators K^+ , K^0 and K^- are the generators of the $su(1,1)$ Lie algebra, and are related to creation and annihilation operators before the quench through the following relations

$$K^+ = \frac{1}{2} \alpha_{ji}^\dagger \alpha_{ji}^\dagger, \quad K^0 = \frac{1}{4} (\alpha_{ji}^\dagger \alpha_{ji} + \alpha_{ji} \alpha_{ji}^\dagger), \quad \text{and} \quad K^- = \frac{1}{2} \alpha_{ji} \alpha_{ji}. \quad (3.8)$$

The generators K_i provide a single-mode bosonic representation of the $su(1,1)$ Lie algebra, and satisfy the usual commutation relations

$$[K_+, K_-] = -2K_0, \quad [K_0, K_\pm] = \pm K_\pm. \quad (3.9)$$

The corresponding Casimir operator, defined as

$$K^2 = K_0^2 - \frac{1}{2} (K_+ K_- + K_- K_+), \quad (3.10)$$

commutes with all the three generators of the algebra, and satisfies the following eigenvalue equation

$$K^2 |m, k\rangle = k(k-1) |m, k\rangle. \quad (3.11)$$

Here the constant k is the Bargmann index of the algebra, and m takes values $0, 1, 2 \dots$. For the single-mode bosonic representation of $su(1, 1)$ Lie algebra given above, the Bargmann index k can take values $1/4$ or $3/4$ (see [66]). For $k = 1/4$, the basis corresponding to a unitary irreducible representation of the algebra is the set of states with an even number of bosons. In this paper, we always consider k to be $1/4$. The operations of the generators K_i on the states $|m, k\rangle$ are given by the usual formulae, which can be found, for example, in [66].

Now using the well known decomposition relations for the $SU(1, 1)$ group elements, the time evolved state after the quench can be written as ²

$$\begin{aligned} |\Psi_f(t)\rangle &= e^{-i\mathcal{H}_f t} |\psi(t=0)\rangle = \exp \left[-2it\omega_{jf} \left(\mathcal{U}_j \mathcal{V}_j K^+ + (\mathcal{U}_j^2 + \mathcal{V}_j^2) K^0 + \mathcal{U}_j \mathcal{V}_j K^- \right) \right] |0\rangle \\ &= \exp \left[\mathbf{X}_+ K^+ \right] \exp \left[\ln \mathbf{X}_0 K^0 \right] \exp \left[\mathbf{X}_- K^- \right] |0\rangle . \end{aligned} \quad (3.12)$$

Here $|0\rangle$ indicates the ground state of the LMG model and the three functions \mathbf{X}_i s are given by

$$\mathbf{X}_\pm = \left(\frac{\mathbf{x}_\pm}{\Theta} \right) \sqrt{\mathbf{X}_0} \sinh \Theta , \quad \mathbf{X}_0 = \left(\cosh \Theta - \frac{\mathbf{x}_0}{2\Theta} \sinh \Theta \right)^{-2} , \quad (3.13)$$

with

$$\mathbf{x}_\pm = -2it\omega_{jf} \mathcal{U}_j \mathcal{V}_j , \quad \mathbf{x}_0 = -2it\omega_{jf} (\mathcal{U}_j^2 + \mathcal{V}_j^2) , \quad \text{and} \quad \Theta^2 = \frac{1}{4} \mathbf{x}_0^2 - \mathbf{x}_+ \mathbf{x}_- . \quad (3.14)$$

It can be seen that since the Hamiltonian is written in terms of the creation and annihilation operators before the quench, which are the elements of the $su(1, 1)$ algebra, the time evolved state is a general $su(1, 1)$ coherent state. For the case of $k = 1/4$, we are considering the scenario when $\mathbf{x}_0 = 0$ and the state reduces to the usual squeezed vacuum state.

Using the decomposed time evolved state in eq. (3.12), we can obtain the auto-correlation function to be

$$\mathcal{S}(t) = \langle \Psi_f(t) | \psi(t=0) \rangle = \left[\cosh \bar{\Theta} + \frac{\mathbf{x}_0}{2\bar{\Theta}} \sinh \bar{\Theta} \right]^{-1/2} , \quad \text{with} \quad \bar{\Theta}^2 = \frac{1}{4} \bar{\mathbf{x}}_0^2 - \bar{\mathbf{x}}_+ \bar{\mathbf{x}}_- , \quad (3.15)$$

and the $\bar{\mathbf{x}}_j$ s are the complex conjugates of \mathbf{x}_j s. Using the expressions for the \mathbf{x}_j s given above, we can rewrite the expression for the auto-correlation as

$$\mathcal{S}(t) = \left[\cos \left[(\mathcal{U}_j^2 - \mathcal{V}_j^2) \omega_{jf} t \right] - i \frac{(\mathcal{U}_j^2 + \mathcal{V}_j^2)}{(\mathcal{U}_j^2 - \mathcal{V}_j^2)} \sin \left[(\mathcal{U}_j^2 - \mathcal{V}_j^2) \omega_{jf} t \right] \right]^{-1/2} . \quad (3.16)$$

This auto correlation function is utilized to obtain Lanczos coefficients in the following subsection.

²See [67] for a derivation of this formula and some other such decompositions in more general scenarios.

3.3 The Lanczos coefficients and the spread complexity

In this subsection, we first compute the Lanczos coefficients using the algorithm described in section 2 from the auto-correlation function given in eq. (3.16). These coefficients can compactly be written as ³

$$a_n = \left(2n + \frac{1}{2}\right) (\mathcal{U}_j^2 + \mathcal{V}_j^2) \omega_{jf} , \text{ with } n = 0, 1, 2, 3, \dots, \quad (3.17)$$

$$\text{and } b_l = \sqrt{2(2l^2 - l)} \mathcal{U}_j |\mathcal{V}_j| \omega_{jf} , \text{ with } l = 1, 2, 3, \dots$$

Notice that the modulus of the quantity \mathcal{V}_j appears in the expression for b_l . This is because for the particular quench model we are considering, \mathcal{V}_j is actually negative in both phases. We explicitly assume that the initial state is always away from the criticality, while the state after the quench is close to the critical point. However, for the case of critical quench considered later, the state after the quench is at the critical point. Since the frequency goes to zero at the critical point, it can be seen from (3.6) that \mathcal{V}_j is negative for such quenches. In this context, we can consider some particular quench protocols where the initial state is close to the QPT. Here also, we can study the evolution of the spread complexity when the initial state is gradually moved towards the critical point. In that case, \mathcal{V}_j changes its sign when ω_{ji} crosses ω_{jf} through successive quenches.

Now using eqs. (2.3) and (3.17), we can find out the elements of the Krylov basis. It can be readily checked that these are the eigen states $|m, k\rangle$ of the Casimir operator K^2 defined in eq. (3.11). For our case, as emphasized before, the state of the system before the quench is the first state of the Krylov basis which makes the subsequent procedure easier to track analytically.

Next we proceed to the calculation of $\phi_n(t)$ s and subsequently, the spread complexity. Following the procedure described in sec. 2, we obtain these to be given by

$$\phi_n(t) = \mathcal{N}_n \phi_0(t) \frac{\mathcal{G}_1(t)^n}{\mathcal{G}_2(t)^n} = \mathcal{N}_n \phi_0(t) \mathcal{G}(t)^n , \quad (3.18)$$

where the time-dependent function $\mathcal{G}(t)$ is defined as

$$\mathcal{G}(t) = \frac{(\omega_{jf}^2 - \omega_{ji}^2) \sin(\omega_{jf} t)}{(\omega_{jf}^2 + \omega_{ji}^2) \sin(\omega_{jf} t) - 2i\omega_{jf}\omega_{ji} \cos(t\omega_{jf})} . \quad (3.19)$$

The quantities \mathcal{N}_n s appearing above are numerical constants. Here we record the first few values for convenience: $\mathcal{N}_0 = 1$, $\mathcal{N}_1 = \frac{1}{\sqrt{2}}$, $\mathcal{N}_2 = \frac{\sqrt{3}}{2\sqrt{2}}$, $\mathcal{N}_3 = \sqrt{\frac{5}{16}}$, $\mathcal{N}_4 = \frac{\sqrt{35}}{8\sqrt{2}}$, \dots

The first important point we note from the expressions for the functions $\phi_n(t)$ s, which hugely simplify the calculation of the complexity is that, the ratio of two successive $\phi_n(t)$ s are related by the following relation ⁴

$$\frac{\phi_{n+1}(t)}{\phi_n(t)} = \frac{\mathcal{N}_{n+1}}{\mathcal{N}_n} \mathcal{G}(t) = \sqrt{\frac{2n+1}{2n+2}} \mathcal{G}(t) . \quad (3.20)$$

³Apart from quantities such as, $\mathcal{U}_j, \mathcal{V}_j$ and ω_{jf} , whose expressions are different in the two phases, we mostly omit the index j in other quantities (such as the Lanczos coefficients) from now on.

⁴With the help of eq. (3.20) it can be easily verified that the condition $\sum_n |\phi_n(t)|^2 = 1$ is satisfied as well.

With this observation, it is easy to write down an exact analytical expression for the spread complexity given in eq. (2.7) as

$$\mathcal{C}(t) = 2|\phi_1(t)|^2 \sum_{n=0}^{\infty} \frac{(n+1)(2n+1)!!}{(2n+2)!!} \mathcal{F}^n(t) = \frac{|\phi_1(t)|^2}{(1-\mathcal{F}(t))^{3/2}}, \text{ where } \mathcal{F}(t) = |\mathcal{G}(t)|^2. \quad (3.21)$$

Here the expression for the time-dependent function $\mathcal{F}(t)$ is given by

$$\mathcal{F}(t) = \frac{(\omega_{jf}^2 - \omega_{ji}^2)^2 \sin^2(\omega_{jf}t)}{(\omega_{jf}^2 + \omega_{ji}^2)^2 \sin^2(\omega_{jf}t) + 4\omega_{jf}^2\omega_{ji}^2 \cos^2(t\omega_{jf})}. \quad (3.22)$$

From the expression for the complexity, we see that for it to be well defined, the function $\mathcal{F}(t)$, and hence the ratio of the modulus squared values of two successive $\phi_n(t)$ s must be smaller than unity at all times. This also provides the reason for the convergence of the infinite sum appearing in the expression for the complexity. Furthermore, the time dependence of the complexities after the quench in both phases of the LMG model is essentially determined by the ratio of the modulus squared of successive ϕ_n s and the modulus of the coefficient of $|K_1\rangle$ in the expansion of the time evolved state.

Finally, using the expression for ϕ_1 from eq. (3.18), the formula for the spread complexity reduces to

$$\mathcal{C}_j(t) = \frac{(\omega_{ji}^2 - \omega_{jf}^2)^2}{8\omega_{jf}^2\omega_{ji}^2} \sin^2(\omega_{jf}t). \quad (3.23)$$

This formula is valid in both phases of the ground state of the LMG model (with $j = 1, 2$ for the broken and the symmetric phase respectively). However, the exact dependence of the complexity on the parameters of the system (h, γ), which are changed during the quench, are different. With the expressions for the frequencies ω_{jf} and ω_{ji} given in eqs. (3.4) and (3.5) we now separately study the time evolution of the spread complexity after the quantum quench in the two phases.

Evolution of complexity in the broken phase of the LMG model

We first assume that the system is prepared at time $t = 0$ in the ground state of the LMG model in the broken phase. The value of h_i is chosen in such a way that it is away from the critical value of the magnetic field, i.e. $h_i < h_c$. At $t = 0$, the parameters h_i, γ_i are suddenly changed to new values h_f, γ_f , and subsequently, the evolution of the system is governed by the new Hamiltonian. We take the magnetic field after the quench h_f to be greater than the initial value h_i , but smaller than the critical value h_c , i.e. $h_i < h_f < h_c$. Thus, the state after the quench is still in the ground state of the final Hamiltonian at the broken phase, but is closer to criticality as compared to the initial state. The special case of critical quench characterized by $h_f = 1$ will be discussed separately in sec. (3.4).

We first study the behavior of the function $\mathcal{F}(t)$ when h_f is gradually taken closer to the critical point. Fig. 1 exhibits oscillatory behavior of the function $\mathcal{F}(t)$ for different values of the post-quench magnetic field h_f , by keeping γ fixed in the broken phase. Here we consider the magnetic field after the quench to be close to the critical value $h_c = 1$, but

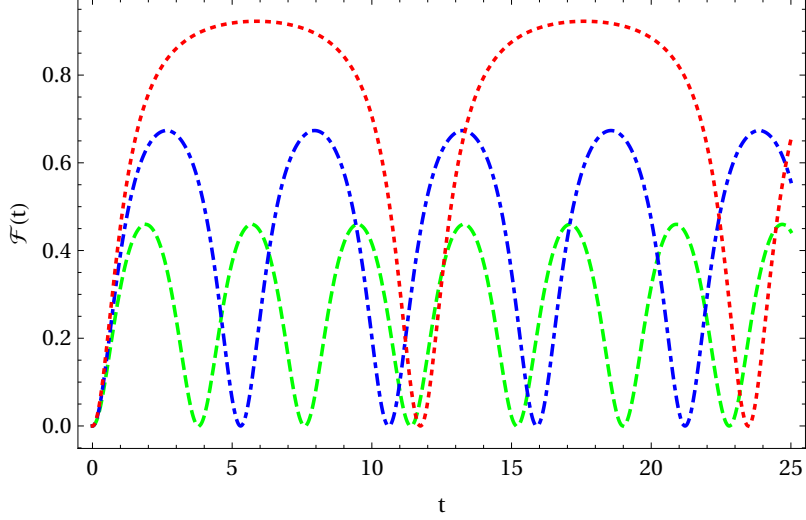


Figure 1: Variation of $\mathcal{F}(t)$ with time in the BP for different post-quench magnetic fields. Here $h_f = 0.9$ (green), $h_f = 0.95$ (blue) and $h_f = 0.99$ (red) respectively. The parameter γ has a fixed value 0.1, and $h_i = 0.5$.

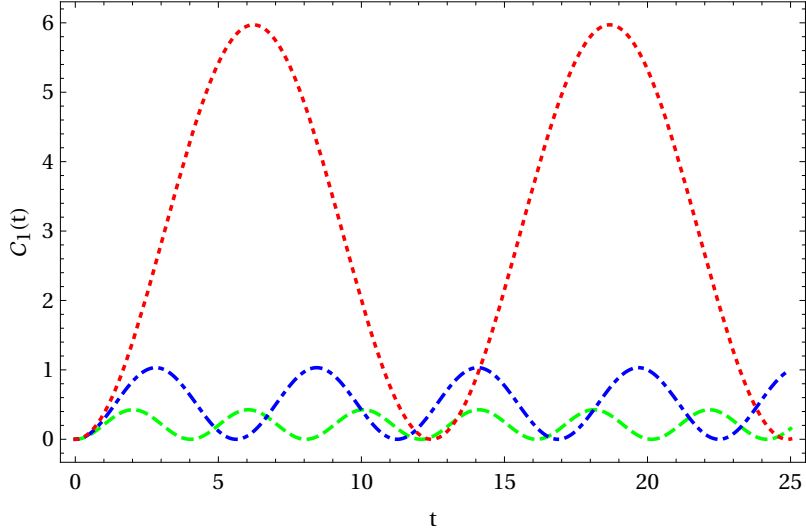


Figure 2: Evolution of $\mathcal{C}_1(t)$ with time in the BP for different post-quench magnetic fields. The parameter values are same as those of Fig. 1.

always less than one. One can see that when h_f gradually approaches the critical point, the amplitude and the time period of the oscillation increase. However, as expected, the function $\mathcal{F}(t)$ is always lower than one.

The expression for the spread complexity after the quench in the broken phase is given by

$$\mathcal{C}_1(t) = \frac{[(1 - h_i^2)(1 - \gamma_i) - (1 - h_f^2)(1 - \gamma_f)]^2}{8(1 - h_i^2)(1 - \gamma_i)(1 - h_f^2)(1 - \gamma_f)} \sin^2 \left(2\sqrt{(1 - h_f^2)(1 - \gamma_f)t} \right). \quad (3.24)$$

This formula is written down for the most general quench with $h_f \neq h_i$ and $\gamma_i \neq \gamma_f$. In the special case when $\gamma_i = \gamma_f$ it can be seen that γ only affects the time period of the oscillations, and not the magnitude. Below we mostly focus on this special case, since in this case the spread complexity carries all the typical characteristics of the general quench.

Time evolution of the spread complexity for the quench protocols considered in Fig. 1 is shown in Fig. 2.⁵ The spread complexity oscillates with time, and the oscillation amplitude and time period gradually increase as the post-quench magnetic field is taken closer to the criticality.

From the formula (2.7), we see that the spread complexity is a weighted sum of the squared modulus of the ϕ_n s. Now, one can notice that the spread complexity increases as the post-quench magnetic field is taken closer to the critical point. Thus, even if we have the exact expression for the infinite sum in eq. (2.7), it is interesting to quantify how many ϕ_n s significantly contribute to the total complexity as the magnetic field moves closer to the critical point.

In the broken phase of the system, when the final magnetic field is far from the critical point, the spread complexity $\mathcal{C}_1(t)$ converges rapidly towards its exact value. Hence, only the first few values of n contribute to the complexity. For example, when $h_f = 0.5$, and $h_i = 0.1$ only the terms $n = 1$ and $n = 2$ have contribution greater than the value 0.00025 towards $\mathcal{C}_1(t)$. On the other hand, when h_f is closer to 1, there is a crossover in the magnitude of individual contributions in eq. (2.7), i.e., there exists a maximum value of n such that the quantities $(n+j)|\phi_{(n+j)}(t)|^2$ are smaller than $n|\phi_n(t)|^2$ for all $j \geq 1$. Since the quantities $n|\phi_n(t)|^2$ are functions of time, by the statement ‘ $(n+j)|\phi_{(n+j)}(t)|^2$ are smaller than $n|\phi_n(t)|^2$ ’, we mean that the maximum values of $(n+j)|\phi_{(n+j)}(t)|^2$ are smaller than the maximum value of $n|\phi_n(t)|^2$. There may be other values of time where $(n+j)|\phi_{(n+j)}(t)|^2$ are actually greater than $n|\phi_n(t)|^2$. However, for sufficiently higher values of j , this statement is applicable for all times. As an example when we set $h_f = 0.99$, with $h_i = 1$, we notice that the individual contribution to the complexity starts to decrease after $n = 10$.⁶

Now we want obtain the effective number of elements $n = N_{eff}$ of the Krylov basis that contribute considerably to the sum in $\mathcal{C}_1(t)$ for different values of h_f close to criticality. We quantify this N_{eff} such that the inequality

$$\mathcal{C}_1^{(N_{eff}+1)}(t) - \mathcal{C}_1^{(N_{eff})}(t) = \sum_{n=0}^{N_{eff}+1} n|\phi_n(t)|^2 - \sum_{n=0}^{N_{eff}} n|\phi_n(t)|^2 \leq \epsilon, \quad (3.25)$$

is satisfied. Here ϵ is a small quantity, which is set to be $\epsilon = 0.001$ in the numerical estimations below.

⁵Unless stated otherwise, we henceforth always set $\gamma_f = \gamma_i = 0.1$ in the plots and any reference of other numerical quantities.

⁶Though the individual terms start to decrease, they may still contribute to the total spread complexity. This is best characterized by the quantity, effective number of elements of the Krylov basis, introduced below.

In Fig. 3 we plot N_{eff} ,⁷ which satisfy the criterion in eq. (3.25), as a function of h_f when h_f is taken close to the criticality. As can be anticipated from the discussion above, N_{max} increases with h_f approaching the criticality. We fitted the data of N_{eff} for different values of h_f with reasonable accuracy and the fitted function is

$$N_{eff}(h_f) = \frac{n_1}{1 - h_f^{n_2}}, \quad (3.26)$$

where in the broken phase, the numerical coefficients have values $n_1 \approx 7.92$ and $n_2 \approx 5.59$. This fitting function (along with the exact result obtained numerically) is shown in Fig. 3 by the red curve. Furthermore, to quantify the growth of N_{eff} with h_f , we also show the plot of the derivative of $N_{eff}(h_f)$ in the inset, which rises sharply towards criticality.

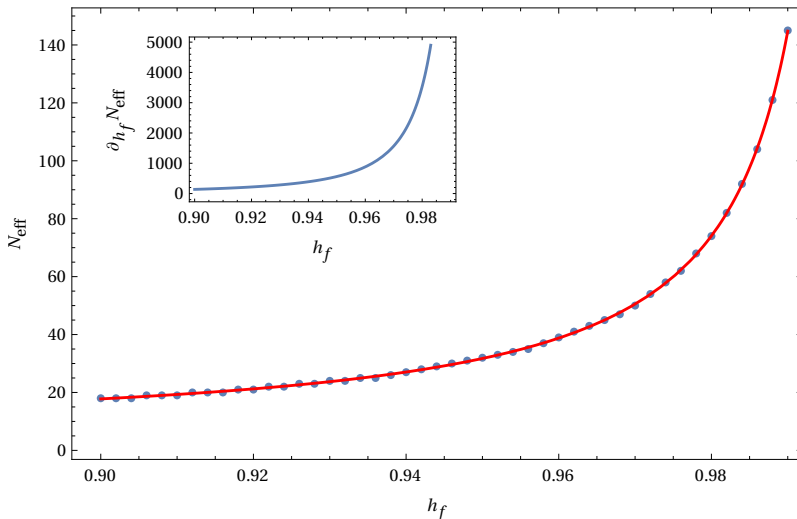


Figure 3: Plot of N_{eff} with h_f close to the criticality in the BP. The blue dots are numerical data which is fitted with the red curve where the equation of the red curve is given in eq. (3.26). The derivative of N_{eff} with respect to h_f is shown in the inset. We set $\epsilon = 0.001$ and $h_i = 0.1$.

In this context we note that, if we take ϵ smaller than the value 0.001 we have used above, there will be a saturation in the estimation of N_{eff} close to the criticality, i.e. there will be ranges of h_f for each of which the quantity N_{eff} will be the same.

Evolution of the complexity in the symmetric phase of the LMG model

Now we assume that the system is prepared in the ground state before the quench at the symmetric phase of the LMG model, with magnetic field $h_i > 1$. The magnetic field after the quench is smaller than h_i and larger than h_c , i.e. $1 < h_f < h_i$. Thus the state of the system after the quench is still in the ground state (of the new Hamiltonian) of the symmetric phase but closer to criticality.

⁷As mentioned in the previous footnote, since $\mathcal{C}(t)$ is a function of time, the criterion in eq. (3.25) is assumed to be implied at the maximum of the complexity.

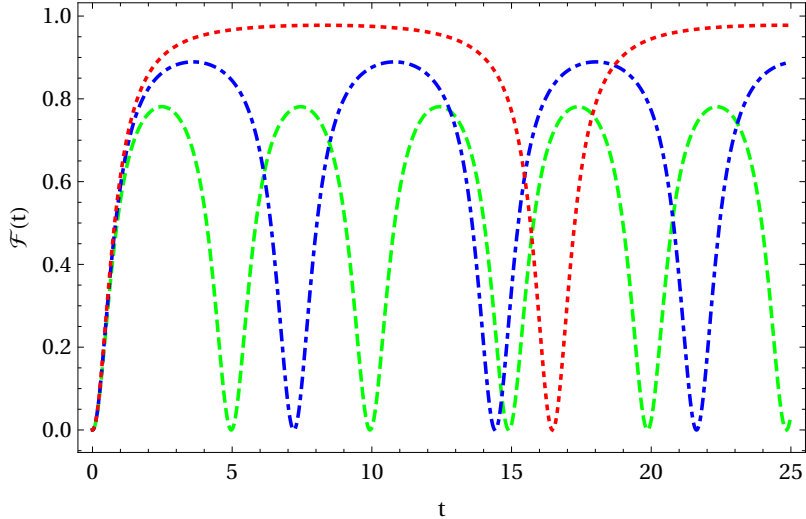


Figure 4: Variation of $\mathcal{F}(t)$ with time in the SP of the system for different post-quench magnetic fields. Here $h_f = 1.1$ (green), $h_f = 1.05$ (blue) and $h_f = 1.01$ (red) respectively. The parameter γ has a fixed value 0.1, and $h_i = 1.5$.

Fig. 4 exhibits the time variation of $\mathcal{F}(t)$ for different values of the post-quench magnetic field h_f , by keeping γ fixed in symmetric phase. The qualitative behavior of this function is similar to that of the one in the broken phase. When the magnetic field values approach the critical point, the peak value of $\mathcal{F}(t)$ gets closer to 1, but always remains smaller than unity.

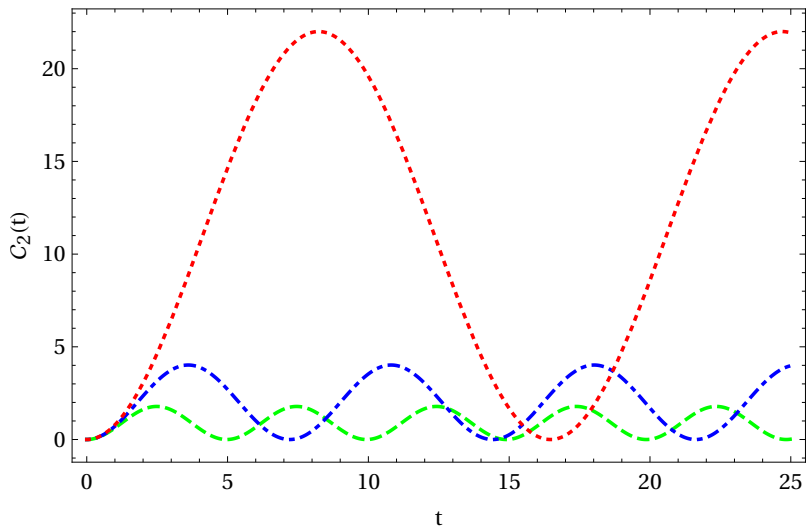


Figure 5: Evolution of $\mathcal{C}_2(t)$ with time for different post-quench magnetic fields in the symmetric phase. The parameter values are same as in Fig. 4.

For quantum quenches in the symmetric phase, the expression for the spread complex-

ity can be written as

$$\mathcal{C}_2(t) = \frac{[(h_i - 1)(h_i - \gamma_i) - (h_f - 1)(h_f - \gamma_f)]^2}{8(h_i - 1)(h_i - \gamma_i)(h_f - 1)(h_f - \gamma_f)} \sin^2 \left(2\sqrt{(h_f - 1)(h_f - \gamma_f)t} \right). \quad (3.27)$$

The dependence of $\mathcal{C}_2(t)$ on γ in this case is different from $\mathcal{C}_1(t)$, namely, for the symmetric phase even when $\gamma_f = \gamma_i$ the anisotropy parameter can affect the magnitude of the spread complexity.

Time evolution of $\mathcal{C}_2(t)$ in the symmetric phase for quenches with different final values of the magnetic field near criticality, is shown in Fig. 5. As h_f approaches towards the critical point, both the amplitude and the time period of oscillations gradually increase.

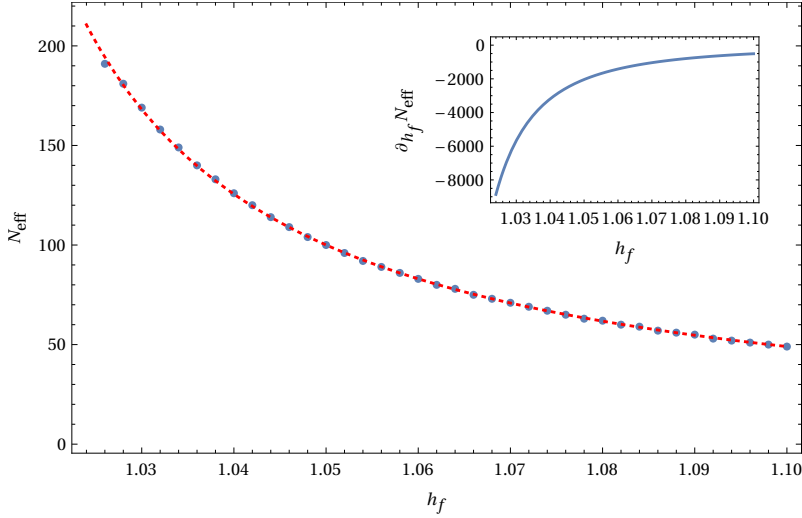


Figure 6: Plot of N_{eff} with h_f close to the criticality in the SP. The fit of the numerical data (blue dots) with eq. (3.26) (red curve). The derivative of N_{eff} with respect to h_f is shown in the inset. Here we set $\epsilon = 0.001$ and $h_i = 0.1$.

Similar to the broken phase, we can quantify the number of terms contributing to the spread complexity expansion up to a preassigned cutoff value. One can check that for magnetic fields which are equally distant from the critical value $h_c = 1$ in the two phases of the ground state, the number N_{eff} that satisfy an equation similar to eq. (3.25) with $\mathcal{C}_1(t)$ replaced by $\mathcal{C}_2(t)$, is greater in the symmetric phase than in the broken phase. Similarly, the crossover of the individual contributions towards the complexity, as described above for the BP, occurs in the SP as well, however for comparatively larger values of n .

The variation of N_{eff} with respect to h_f taken closer to the critical point is shown in Fig. 6, along with the fitting function in eq. (3.26) indicated by the red dashed curve. Here the numerical constant have values $n_1 \approx -9.36$ and $n_2 \approx -1.83$ for the best fit of the numerical data. From the derivative of N_{eff} shown in the inset of this figure, we see that close to the criticality, the increase of N_{eff} is sharper compared to the broken phase. Thus we conclude that, as we approach the critical point using quenches in the symmetric phase, the time evolved wavefunctions after quench spread over a larger number of elements of the Krylov basis compared to the symmetrically performed quenches in the broken phase.

3.4 Complexity evolution after a critical quench and dependence on the initial state

Next we study the behavior of complexity for the critical quench, i.e. we assume that the post-quench magnetic field $h_{jf} = 1$, in either of the two phases. Taking the limit $\omega_{jf} \rightarrow 0$, we see from eq. (3.23) that for the critical quench the complexity grows with time as

$$\mathcal{C}_j(t)|_{h_{jf}=1} = \frac{\omega_{ji}^2}{8} t^2. \quad (3.28)$$

Now for critical quenches starting from arbitrary values of the magnetic fields h_{ji} , the values of the ω_{ji} s are not equal. Hence we observe different behavior of the spread complexity in the two phases. In particular, in the broken phase, with an arbitrary initial magnetic field h_{1i} , the time evolution of complexity is different from that of in the symmetric phase with the initial magnetic field $h_{2i} (\neq h_{1i})$. In the following, we consider the time evolution of the spread complexity at the critical quench for different initial magnetic fields, equal distances away from the critical value.

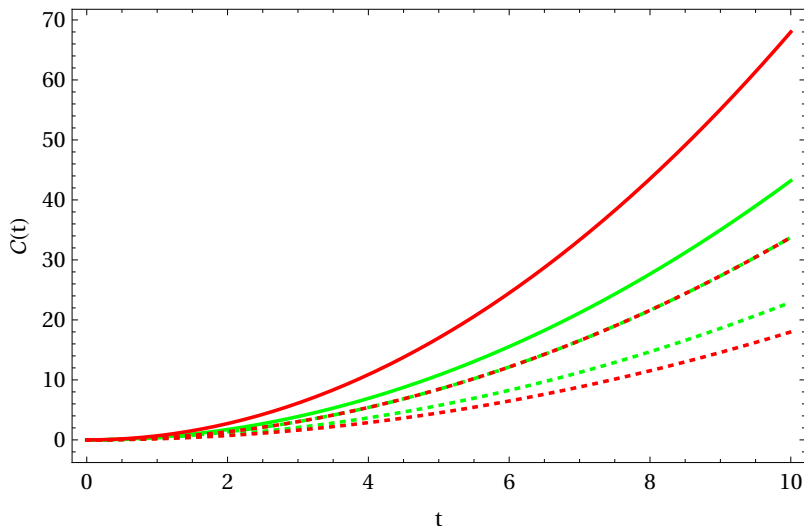


Figure 7: Evolution of $\mathcal{C}(t)$ in either phase of the system for critical quenches with different initial states. Solid red and green curves are with $h_i = h_c \pm 0.8$, dotted red and green are with $h_i = h_c \pm 0.3$. For a given h_{1i} we can obtain a h_{2i} for which the complexities coincides. This is shown here with $h_{1i} = 0.5$, for which we can find $h_{2i} = 1.486$ for the crossover of complexities (dashed red and green curves). We have used $\gamma = 0.1$.

Fig. 7 depicts the effect of changing the initial magnetic field on the critical quench. When the magnetic fields are far away from the critical point, the complexity in the symmetric phase (solid red curve) grows faster than the one in the broken phase (solid green curve). However, when the initial magnetic fields take values closer to the critical point, the complexity in the broken phase (dotted green curve) grows faster than the symmetric phase (dotted red curve). Thus, one can notice that for a given h_{1i} , there is a particular value of h_{2i} for which the time evolution of the complexities are identical in both phases.

In particular, this happens when the two initial frequencies ω_{ji} s are equal. In that case, we can conclude that the complexity evolution is continuous across the two phases.

An analytical formula for the relation between h_{1i} and h_{2i} can be derived from the expression for complexity in the critical quench derived above. This can be checked to be given by

$$h_{2i} = \frac{1}{2} \left(\gamma + 1 + \sqrt{(1 - \gamma)(5 - 4h_{1i}^2 - \gamma)} \right). \quad (3.29)$$

An example of such evolution is shown in Fig. 7 with $h_{1i} = 0.5$ being the initial magnetic field in the broken phase. Utilizing the eq. (3.29), we can obtain the initial magnetic field in the symmetric phase $h_{2i} = 1.486$ for the evolution to be identical in both phases after a critical quench.

Before concluding this section, we note that quadratic evolution of the complexity is a typical behavior shown by the complexity of the free particle [56]⁸. In the thermodynamic limit, the Hamiltonian of the LMG model can be expressed as a harmonic oscillator with a vanishing frequency after the critical quench; hence, the system becomes a free particle. This provides a straightforward explanation of the quadratic growth of complexity after a critical quench.

4 Time Evolution of spread entropy

In this section, we study another interesting quantity relevant in the context of the wave function spread over the Krylov basis, namely the spread entropy which is defined as [35]

$$S_K = - \sum_n |\phi_n(t)|^2 \log |\phi_n(t)|^2. \quad (4.1)$$

Utilizing the expressions for ϕ_n s obtained in the eq. (3.18), we can express the spread entropy as follows

$$S_K(t) = -|\phi_0(t)|^2 \left[\sum_n \mathcal{N}_n^2 \mathcal{F}^n(t) \ln(\mathcal{N}_n^2) + \ln(|\phi_0(t)|^2) \sum_n \mathcal{N}_n^2 \mathcal{F}^n(t) + \ln(\mathcal{F}(t)) \sum_n n \mathcal{N}_n^2 \mathcal{F}^n(t) \right]. \quad (4.2)$$

Here the numerical constants \mathcal{N}_n are given by

$$\mathcal{N}_n = \frac{\Gamma(n + \frac{1}{2})}{\sqrt{\pi} \Gamma(n + 1)}. \quad (4.3)$$

with the above equation, we can express the second and third term of the eq. (4.2) in a compact form. Now the spread entropy can be written as ,

$$S_K(t) = -|\phi_0|^2 \left[\sum_{n=1}^{\infty} \mathcal{N}_n^2 \mathcal{F}^n \ln(\mathcal{N}_n^2) + \frac{\ln(|\phi_0|^2)}{\sqrt{1 - \mathcal{F}}} + \frac{\mathcal{F} \ln(\mathcal{F})}{2(1 - \mathcal{F})^{3/2}} \right]. \quad (4.4)$$

⁸Note that a general argument was presented in [56] supporting the quadratic growth of the complexity.

Since the first term in eq. (4.2) does not offer any simple expression, we will study its behavior separately.

In Fig. 8, we plot the ratio of the numerical coefficients of the successive terms in the first summation above. It can be observed that the ratio $\frac{T_{n+1}}{T_n}$ has a value greater than unity only for $n = 1$ whereas for higher values of n , it approaches a constant value around 1. On the other hand it was shown that the function $\mathcal{F}(t)$ is always smaller than 1 for

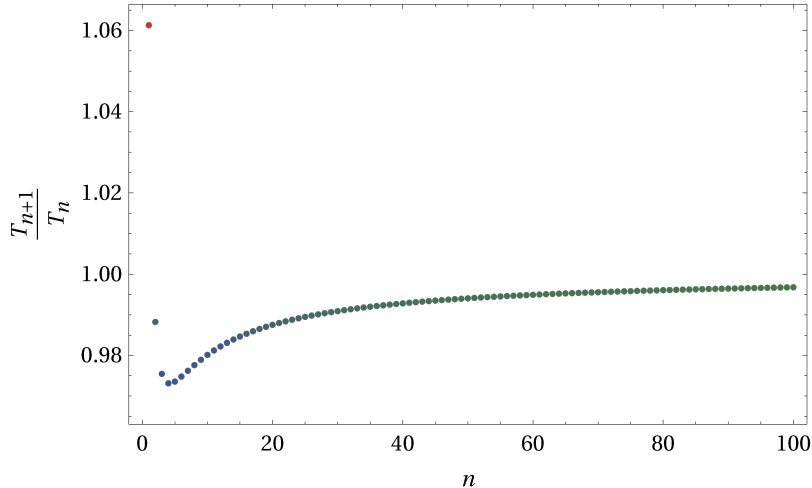


Figure 8: Plot of the ratio $\frac{\mathcal{N}_{n+1}^2 \ln(\mathcal{N}_{n+1}^2)}{\mathcal{N}_n^2 \ln(\mathcal{N}_n^2)}$. For higher values of n the ratio approaches to a limiting value of 0.995

non-critical values of the magnetic field (see Figs. 1, 4). Hence for the quench scenarios under consideration, the infinite sum can be replaced by the sum of a finite number of terms with an excellent accuracy. This fact will help us study the evolution of spread entropy in the next section.

4.1 Post-quench evolution of spread entropy

In this section, we study the evolution of the spread entropy after a quantum quench in the broken phase and the symmetric phases, away from the criticality as well as at the critical point of the LMG model. Special emphasis is given on the behavior of the first term (the infinite sum) in eq. (4.4), which we call T_1 for convenience.

First we analyze the broken phase of the ground state when the system is away from the critical point. In Fig. 9, the red and the green curves show the time variation of T_1 , considering the sum of first two and thirty terms respectively. The identical character of these two curves for all values of time indicate that the contributions from the terms with higher values of n are negligible. The inset of Fig. 9 shows that the contribution of the second term is much smaller compared to the first term. Hence we claim that the infinite sum is rapidly convergent and its value at any instant of time can be replaced by the sum of its first two terms when the system is in broken phase and is sufficiently away from the critical point.

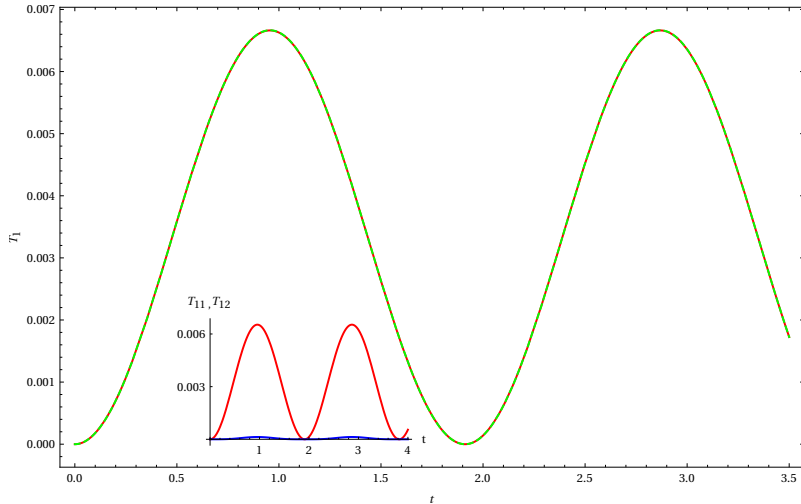


Figure 9: Plot of T_1 , the first term in the expression for the spread entropy. The red curve is sum of first two terms, while the green dashed curve is sum of first 30 terms. Two plots are also identical implying that the sum converges rapidly. Here $h_f = 0.5, h_i = 0.1, \gamma_f = \gamma_i = 0.1$. The inset shows the contribution of the $n = 1$ term (called T_{11}) and $n = 2$ th term (called T_{12}) term in T_1 .

Now we consider different values of h_f to probe the sensitivity of $S_K(t)$. In Fig. 10, we plot the spread entropy for two different values of the magnetic fields, $h_f = 0.5$ and $h_f = 0.7$ respectively where $h_i = 0.1$. Here we observe that the sum T_1 collects considerable amount of contributions from the terms with higher values of n as we take the magnetic field closer to the critical value⁹. As an example, we set $h_f = 0.7$ which is close to critical value compared to $h_f = 0.5$. The time variation of the spread complexity with $h_f = 0.7$ is shown in Fig. 10 (green dashed line) where only the first three terms have any meaningful contribution to T_1 in sense of an equation analogues to eq. (3.25), defined for the spread entropy. Furthermore, it can also be checked that the third term in eq. (4.4) has the dominant contribution in $S_K(t)$ where the first term contributes the least.

Now we analyze the scenario where the post-quench magnetic field value is very close to the critical point. It is observed that the terms with higher values of n which contributes to T_1 increases rapidly. For $h_f = 0.99$ the infinite sum T_1 saturates after summing up to 70 terms, while for $h_f = 0.999$ this number goes up to 300. The time evolution of the spread entropy for these two post-quench magnetic fields are plotted simultaneously in Fig. 11.

For quench in the symmetric phase, similar qualitative behavior of the spread entropy can be observed. However, the quantitative behavior between these two cases are different. Specifically, the number of terms which contributes towards the sum T_1 , such that, even by adding the next term T_1 does not increase more than $\epsilon = 0.001$ are not equal.¹⁰

For example, when we take $h_f = 1.5$ at least terms with $n = 1, 2, 3$ have considerable

⁹As we have discussed previously, this is of course true for the time evolution of the spread complexity as well.

¹⁰Once again this statement is made by looking at the maxima of these time varying functions.

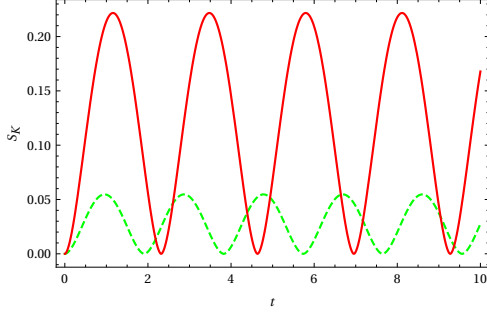


Figure 10: Plot of the time variation of the spread entropy in the broken phase, when the magnetic field is away from critical point. Here, $h_f = 0.5$ (green) and $h_f = 0.7$ (red), and $h_{1i} = 0.1$.

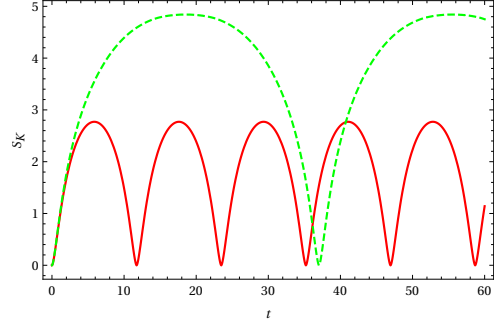


Figure 11: Plot of the time variation of the spread entropy in the broken phase, when the magnetic field is close to the criticality. Here, $h_f = 0.99$ (red) and $h_f = 0.999$ (green), and $h_{1i} = 0.1$.

amount of contribution in the sum.¹¹ Analyzing the system close to the critical point i.e. $h_f = 1.01$, we have to sum up to 175 terms to reach the saturation of T_1 . Following the above discussion, we conclude that in the symmetric phase the infinite sum T_1 converges slowly compared to the broken phase.

4.2 Evolution of spread entropy in the critical quench

In this section, we study the evolution of spread entropy $S_{Kc}(t)$, in the regime of critical quench. Considering the limit $\omega_{jf} \rightarrow 0$, we can express the three terms in eq. (4.4) as follows (denoting them as T_1, T_2 and T_3 for convenience),

$$\begin{aligned}
 T_1(t)|_{\omega_{jf} \rightarrow 0} &= -2 \sum_{n=1}^{\infty} \mathcal{N}_n^2 \ln(\mathcal{N}_n^2) \frac{(\omega_{ji}^2 t^2)^n}{(4 + \omega_{ji}^2 t^2)^{n+1/2}}, \\
 T_2(t)|_{\omega_{jf} \rightarrow 0} &= -\frac{1}{2} \ln \left[\frac{4}{4 + \omega_{ji}^2 t^2} \right], \\
 T_3(t)|_{\omega_{jf} \rightarrow 0} &= -\frac{\omega_{ji}^2 t^2}{8} \ln \left[\frac{\omega_{ji}^2 t^2}{4 + \omega_{ji}^2 t^2} \right].
 \end{aligned} \tag{4.5}$$

We define a dimensionless parameter $x = \omega_{ji}t$ which controls the behavior of T_1, T_2 and T_3 in broken and symmetric phase. For small x , the spread entropy rises sharply in the initial time, then after reaching a peak value it starts to decrease, until it hits a minimum and finally at late time it diverges. The time at which the peak of $S_{Kc}(t)$ is reached can be determined by the frequency ω_{ji} , and hence, by the value of the initial magnetic field h_{ji} . For small values of ω_{ji} , the peaks appear at later times and the spread entropy diverges less rapidly at late times compared to the larger ω_{ji} s.

¹¹Note that, in the broken phase, T_1 received the major contributions only from the first and the second term where the magnetic field was $h_f = h_c - 0.5$. All these statements are made by assuming a cutoff of $\epsilon \approx 0.001$.

In Fig. 12, we present the time evolution of the critical spread entropy ($S_{Kc}(t)$) for two different values of the magnetic fields in the symmetric phase. To explain the behavior the plots, we analyze the early and late time characteristics separately for each of the terms in eq. (4.5).

For small values of x (with fixed ω_{ji}), all the terms in eq. (4.5) have the lowest order contributions as $T_1 \approx \frac{\ln 2}{8} x^2$, $T_2 \approx \frac{x^2}{8}$, and $T_3 \approx -\frac{x^2}{8} \ln \left[\frac{x^2}{4} \right]$. Following these contributions, it is observed that the third term offers the dominant contribution in the growth of the spread entropy at early times just after the quench. On the other hand, at late times T_1 , T_2 and T_3 show different behavior. The first term T_1 , reaches a peak value and then decays to zero at late times, with the decay rate depending on the frequency ω_{ji} . The second term, grows continuously after the quench and at late times it diverges logarithmically, with the rate of growth depending on the initial frequency. Finally, the third term after the initial growth, saturates to a constant value $1/2$ at the limit $x \rightarrow \infty$ irrespective of the frequency ω_{ji} .

Taking the initial magnetic field to be close to the final magnetic field (which is equal to unity here), the critical spread entropy shows a slow increase up to a peak value and then falls off slowly compared to the plot where the initial magnetic field is away from the final value. The rate of growth at late times is also slow in this case. In both the cases shown in Fig. 12, we have taken sum of first 900 terms to compute T_1 which provides an excellent convergence for small values of t . However, for large t this is slightly inaccurate. It can be checked that the contribution of T_1 towards $S_{Kc}(t)$ is much smaller compared to the second term. At late times, T_2 shows logarithmic divergence which becomes the dominant contribution in $S_{Kc}(t)$. Thus, the restriction in the accurate computation of T_1 does not affect the results presented here.

Similar behavior of the critical spread entropy as shown in Fig. 12 can also be observed for quench in the broken phase of the system. Furthermore, for a given magnetic field in the broken phase, we can obtain a particular value of the magnetic field where the evolution of critical spread entropies are identical in two phases. Note that a similar behavior was observed in eq. (2.7) for spread complexity.

5 Conclusions

In this paper, we have used the spread complexity as a probe of equilibrium quantum phase transition when a system is quenched towards the critical point. We have defined a novel quantity named effective basis (N_{eff}), which measures the number of elements of the Krylov basis contributing significantly to the sum of spread complexity. We have shown that this grows rapidly as the post-quench magnetic field is driven towards the critical point from both phases. We argue that this measure of effective basis can also distinguish between two phases of the LMG model as the natures of growth in the two phases are different. In the context of critical quench, we have shown that the spread complexity grows in a quadratic manner with time, which agrees with the results available in the literature. This behavior of the spread complexity can be expected, since the system at

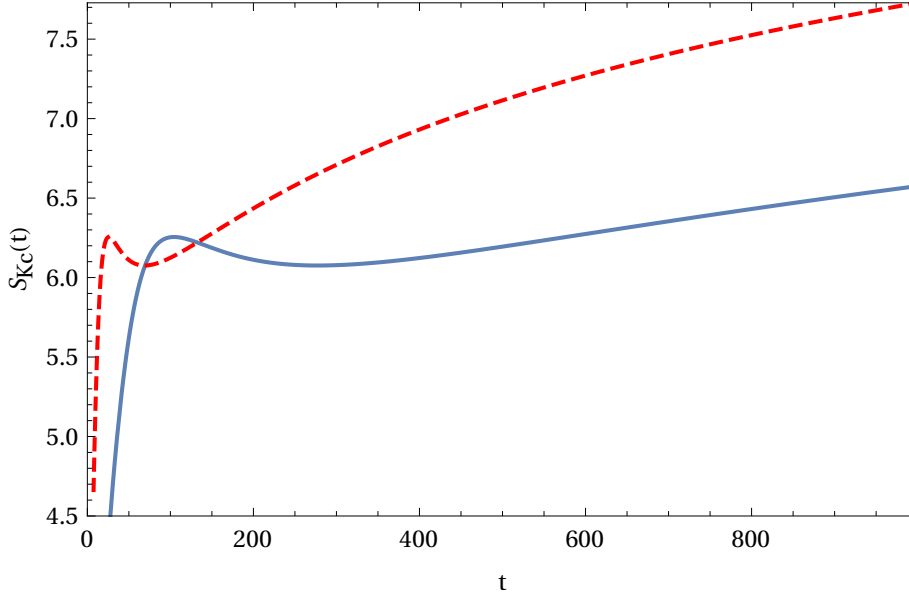


Figure 12: Time variation of spread entropy after a critical quench in the symmetric phase. The red curve is with $h_i = 1.9$ ($\omega_i \approx 2.545$) and the blue curve is for $h_i = 1.1$ ($\omega_i \approx 0.632$).

the critical quench behaves like a free particle. This is in accordance with the arguments given in [56].

A similar analysis for spread entropy reveals an oscillatory behaviour when the final value of the magnetic field is away from the critical point in both phases. On the other hand, near criticality, the spread entropy still exhibits an oscillatory behavior but with a larger amplitude and time period. However, in the symmetric phase, the infinite sum in the spread entropy converges slowly compared to the broken phase.

In this paper, we have taken a first step towards understanding the quantum phase transition from the viewpoint of spread complexity. For the model chosen, it was possible to write down the Lanczos coefficients explicitly, and the resulting sum is convergent towards a finite value. However, this is not guaranteed to happen for more complicated models, and an appropriate regularization procedure might be needed. Consequently, many of the features that appeared in our case might be altered, and we leave this kind of analysis at this point for future works.

Acknowledgements

We sincerely thank Diptarka Das, Suchetan Das, and Tapobrata Sarkar for discussions and their valuable comments on a draft version of this manuscript. We also acknowledge MHRD, India for Research Fellowship. BD would also like to acknowledge the support provided by Max Planck Partner Group grant MAXPLA/PHY/2018577. We also remember the fond memories of “Hall-X corridors” where the main idea of this article was generated and many of the discussions took place.

A Spread complexity in quantum quench of the SSH model

In this appendix we briefly describe the time evolution of the spread complexity in the quantum quenches of the Su-Schrieffer-Heeger (SSH) model, when the state before the quench is taken to be the first state of the Krylov basis (which in the context of the SSH model is the lowest weight state of a $su(2)$ representation). In this case, only finite number of Lanczos coefficients a_n and b_n are non-zero in a quench profile, and as a result only finite numbers of terms contribute in the sum (2.7) in the definition of the spread complexity. This is in contrast with the LMG model considered in the main text, where, as we have seen, there are infinite number of non-zero Lanczos coefficients a_n and b_n , and hence the spread complexity is an infinite sum of non-zero terms. As we show, depending on this difference in the behavior of the Lanczos coefficients, time evolution of the spread complexities show different characteristics in the two cases.

We consider a simplified version of the SSH model given by the following Hamiltonian, written in terms of two-flavored fermion creation and annihilation operators $(\alpha_i, \alpha_i^\dagger)$ and $(\beta_i, \beta_i^\dagger)$ as,

$$\mathcal{H} = q_1 \sum_k \left(\alpha_i^\dagger \beta_i + h.c. \right) - q_2 \sum_k \left(\beta_i^\dagger \alpha_{i+1} + h.c. \right). \quad (\text{A.1})$$

Here, we shall assume that the two parameters q_1 and q_2 take only real positive values $q_1 \geq 0$ and $q_2 \geq 0$. The system exhibits two different phases depending on the relative values of these two parameters, namely, when $q_1 > q_2$ the system is in the non-topological phase, whereas, when $q_1 < q_2$ the system is in the topological phase. These two phases are separated by a critical point at $q_1 = q_2$.

In the momentum space, the Hamiltonian of the SSH model written above can be written as [68]

$$\mathcal{H} = \sum_k \left[2r_3 J_0^{(k)} + ir_1 \left(J_+^{(k)} - J_-^{(k)} \right) \right]. \quad (\text{A.2})$$

Here, the coefficients r_i are related to the original parameters q_i s by the following relations [68]

$$r_1 = q_1 - q_2 \cos k, \quad \text{and} \quad r_3 = q_2 \sin k, \quad (\text{A.3})$$

and $J_i^{(k)}$ are the generators of the $su(2)$ algebra, which satisfy the usual commutation relations for each momentum mode. In the momentum space, the SSH Hamiltonian we have considered, is thus an element of the $su(2)$ algebra, and hence the ground state of the system is actually direct product of spin coherent states corresponding to each modes [57]. For future convenience we define an angle θ_k as

$$\sin \theta_k = \frac{|r_1|}{r}, \quad \cos \theta_k = \frac{r_3}{r}, \quad \text{with} \quad r = \sqrt{r_1^2 + r_3^2} = \sqrt{q_1^2 + q_2^2 - 2q_1 q_2 \cos k}. \quad (\text{A.4})$$

To study the time evolution of the spread complexity in the SSH model we consider the following quench protocol. We assume that before quench the system is prepared in state $|\frac{1}{2}, -\frac{1}{2}\rangle$, which is a direct product of the states of the form $|\frac{1}{2}, -\frac{1}{2}\rangle_k$. Each of these states $|\frac{1}{2}, -\frac{1}{2}\rangle_k$ is annihilated by the operator $J_-^{(k)}$. This state is the first state of the Krylov basis i.e. $|K_0\rangle = |\frac{1}{2}, -\frac{1}{2}\rangle$. At $t = 0$ we instantaneously change the parameters q_1^i, q_2^i before

the quench to a new set of values q_1^f, q_2^f . The subsequent time evolution of the system is generated by the new Hamiltonian \mathcal{H}_f corresponding to these new set of parameters.

Before delving into the calculation of the spread complexity in such a quench protocol we notice the following important point. The spread complexity in a quantum quench protocol of the SSH model we are considering has been studied recently in [57]. However in that work the state of the system before the quench is assumed to be the ground state of the initial Hamiltonian, so that the first element of the Krylov basis is not the same as the state before the quench. On the other hand we have assumed that the initial state is the lowest weight state of the $SU(2)$ group, which is not the ground state of the system. After computing the spread complexity we shall compare the two results.

Let us first study the time evolved state after the quench, given for each momentum mode as

$$|\Psi_k(t)\rangle = \exp \left[-it \left(2r_{3f} J_0^{(k)} + ir_{1f} (J_+^{(k)} - J_-^{(k)}) \right) \right] \left| \frac{1}{2}, -\frac{1}{2} \right\rangle_k . \quad (\text{A.5})$$

Using the well known decomposition formula for the $SU(2)$ group elements (see for example [67] for derivations of such formulas) we can easily see that the time evolved state is a linear combination of only two basis elements, namely ¹² $|\frac{1}{2}, -\frac{1}{2}\rangle$ and $|\frac{1}{2}, \frac{1}{2}\rangle$. Essentially, these are the elements of the Krylov basis. Thus it can be anticipated that only finite numbers of Lanczos coefficients can have nonzero values. This fact also makes the calculation of the spread complexity much simpler.

Using this time evolved state we can calculate auto-correlation function $\mathcal{S}(t)$ as

$$\mathcal{S}_{SSH}(t) = \langle \Psi_f(t) | \psi(t=0) \rangle = \cos(r_f t) - i \cos \theta_f \sin(r_f t) . \quad (\text{A.6})$$

We first notice that this is different from the one obtained in [57]. In particular, $\mathcal{S}_{SSH}(t)$ given above does not depend on the parameters of the initial Hamiltonian. However this is expected since we have assumed the system to be prepared in the state $|\frac{1}{2}, -\frac{1}{2}\rangle$, which is not the ground state of the system, and hence does not depend on the parameters of the initial Hamiltonian.

Using the Lanczos algorithm we can calculate the non-zero Lanczos coefficients in this case to be

$$a_0 = -r_f \cos \theta_f , \quad a_1 = r_f \cos \theta_f , \quad \text{and} \quad b_1 = r_f |\sin \theta_f| . \quad (\text{A.7})$$

Next, we write down the expansion coefficients $\phi_0(t)$ and $\phi_1(t)$ of the time evolved state in the Krylov basis:

$$\phi_0(t) = \cos(r_f t) + i \cos \theta_f \sin(r_f t) , \quad \text{and} \quad \phi_1(t) = -i |\sin \theta_f| \sin(r_f t) . \quad (\text{A.8})$$

Using these we obtain the expression for the spread complexity of a single momentum mode, written in terms of the parameters of the SSH model, to be given by

$$\mathcal{C}_k(t) = \frac{(q_1^f - q_2^f \cos k)^2}{(q_1^f)^2 + (q_2^f)^2 - 2q_1^f q_2^f \cos k} \sin^2 \left(\left[(q_1^f)^2 + (q_2^f)^2 - 2q_1^f q_2^f \cos k \right] t \right) . \quad (\text{A.9})$$

In the continuum limit the total complexity is obtained by integrating over the entire range of k and multiplying by a factor of 2, accounting for the negative k modes.

¹²There may be a normalization factor difference from these basis states.

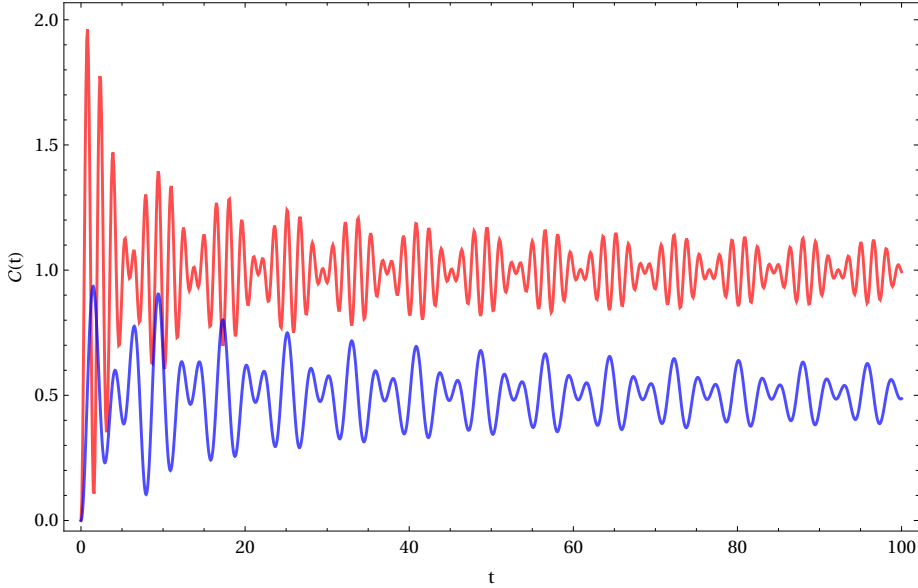


Figure 13: Time evolution of spread entropy after quench in the SSH model. The red curve is with $q_1^f = 2, q_2^f = 0.2$, and the blue curve is with $q_1^f = 0.2, q_2^f = 1$.

In Fig. 13 we have shown the time evolution of the spread complexity after quantum quenches in the SSH model for two different final states obtained by numerically integrating the expression for the complexity for each mode obtained above. The red plot shows the time evolution when the post-quench state is in the non-topological phase, while the blue curve indicates the evolution when the final state is in the topological phase. The general behavior of the complexity is oscillatory with decaying magnitude, and after a sufficient amount of time after the quench the complexity of the non-topological phase is always larger than the topological phase. Thus if we perform two different quenches of the parameters of the SSH model where, in the first case the final state is in the non-topological phase, while in the second case the final state is in the topological phase then using the evolution curves for the spread complexity under these different quench protocols we can distinguish the two phases of the SSH model.

We also notice that the time period of oscillations of $\mathcal{C}_k(t)$ remains unchanged if we interchange the values of q_1^f with q_2^f , only their magnitude will be different. Though the general oscillatory behavior of the spread complexity in our case is the same as the one obtained in [57], there is one difference. If we consider two quench protocols where the final states are in two different phases with the two parameters are being just interchanged, then in our case the complexity oscillates around two different values, while according to the results of [57] the complexity oscillates around a common value irrespective of the final phase of the system. It would be interesting to quantify this difference further.

References

- [1] L. Susskind, *Computational Complexity and Black Hole Horizons*, *Fortsch. Phys.* **64** (2016) 24 [[1403.5695](#)]. 1
- [2] M.A. Nielsen, *A geometric approach to quantum circuit lower bounds*, [0502070](#). 1
- [3] R. Jefferson and R.C. Myers, *Circuit complexity in quantum field theory*, *JHEP* **10** (2017) 107 [[1707.08570](#)]. 1
- [4] R. Khan, C. Krishnan and S. Sharma, *Circuit Complexity in Fermionic Field Theory*, *Phys. Rev. D* **98** (2018) 126001 [[1801.07620](#)]. 1
- [5] A. Bhattacharyya, A. Shekar and A. Sinha, *Circuit complexity in interacting QFTs and RG flows*, *JHEP* **10** (2018) 140 [[1808.03105](#)]. 1
- [6] S. Chapman, M.P. Heller, H. Marrochio and F. Pastawski, *Toward a Definition of Complexity for Quantum Field Theory States*, *Phys. Rev. Lett.* **120** (2018) 121602 [[1707.08582](#)]. 2
- [7] R.-Q. Yang and K.-Y. Kim, *Complexity of operators generated by quantum mechanical Hamiltonians*, *JHEP* **03** (2019) 010 [[1810.09405](#)]. 2
- [8] L. Hackl and R.C. Myers, *Circuit complexity for free fermions*, *JHEP* **07** (2018) 139 [[1803.10638](#)]. 2
- [9] S. Chapman, J. Eisert, L. Hackl, M.P. Heller, R. Jefferson, H. Marrochio et al., *Complexity and entanglement for thermofield double states*, *SciPost Phys.* **6** (2019) 034 [[1810.05151](#)]. 2
- [10] G. Di Giulio and E. Tonni, *Subsystem complexity after a global quantum quench*, *JHEP* **05** (2021) 022 [[2102.02764](#)]. 2
- [11] A. Bhattacharyya, P. Caputa, S.R. Das, N. Kundu, M. Miyaji and T. Takayanagi, *Path-Integral Complexity for Perturbed CFTs*, *JHEP* **07** (2018) 086 [[1804.01999](#)]. 2
- [12] J. Erdmenger, M. Gerbershagen and A.-L. Weigel, *Complexity measures from geometric actions on Virasoro and Kac-Moody orbits*, *JHEP* **11** (2020) 003 [[2004.03619](#)]. 2
- [13] P. Basteiro, J. Erdmenger, P. Fries, F. Goth, I. Matthaiakakis and R. Meyer, *Quantum Complexity as Hydrodynamics*, [2109.01152](#). 2
- [14] S. Chapman and G. Policastro, *Quantum computational complexity from quantum information to black holes and back*, *Eur. Phys. J. C* **82** (2022) 128 [[2110.14672](#)]. 2
- [15] F. Liu, S. Whitsitt, J.B. Curtis, R. Lundgren, P. Titum, Z.-C. Yang et al., *Circuit complexity across a topological phase transition*, *Phys. Rev. Res.* **2** (2020) 013323 [[1902.10720](#)]. 2
- [16] S. Sachdev, *Quantum Phase Transitions*, *C.U.P.*, 1999, . 2
- [17] Z. Xiong, D.-X. Yao and Z. Yan, *Nonanalyticity of circuit complexity across topological phase transitions*, *Phys. Rev. B* **101** (2020) 174305 [[1906.11279](#)]. 2
- [18] N. Jaiswal, M. Gautam and T. Sarkar, *Complexity and information geometry in the transverse XY model*, *Phys. Rev. E* **104** (2021) 024127 [[2005.03532](#)]. 2
- [19] N. Jaiswal, M. Gautam and T. Sarkar, *Complexity, information geometry, and Loschmidt echo near quantum criticality*, *J. Stat. Mech.* **2207** (2022) 073105 [[2110.02099](#)]. 2
- [20] G. Camilo and D. Teixeira, *Complexity and Floquet dynamics: Nonequilibrium Ising phase transitions*, *Phys. Rev. B* **102** (2020) 174304 [[2009.00069](#)]. 2

- [21] U. Sood and M. Kruczenski, *Circuit complexity near critical points*, *J. Phys. A* **55** (2022) 185301 [2106.12648]. 2
- [22] W.-H. Huang, *Complexity of Bose-Hubbard Model : Quantum Phase Transition*, 2112.13066. 2
- [23] K. Pal, K. Pal and T. Sarkar, *Complexity in the Lipkin-Meshkov-Glick Model*, 2204.06354. 2, 3
- [24] D.W.F. Alves and G. Camilo, *Evolution of complexity following a quantum quench in free field theory*, *JHEP* **06** (2018) 029 [1804.00107]. 2
- [25] H.A. Camargo, P. Caputa, D. Das, M.P. Heller and R. Jefferson, *Complexity as a novel probe of quantum quenches: universal scalings and purifications*, *Phys. Rev. Lett.* **122** (2019) 081601 [1807.07075]. 2
- [26] T. Ali, A. Bhattacharyya, S. Shajidul Haque, E.H. Kim and N. Moynihan, *Time Evolution of Complexity: A Critique of Three Methods*, *JHEP* **04** (2019) 087 [1810.02734]. 2, 8
- [27] K. Pal, K. Pal, A. Gill and T. Sarkar, *Evolution of circuit complexity in a harmonic chain under multiple quenches*, 2206.03366. 2
- [28] M. Gautam, N. Jaiswal, A. Gill and T. Sarkar, *Complexity and quenches in models with three and four spin interactions*, 2207.14090. 2
- [29] T. Ali, A. Bhattacharyya, S.S. Haque, E.H. Kim, N. Moynihan and J. Murugan, *Chaos and Complexity in Quantum Mechanics*, *Phys. Rev. D* **101** (2020) 026021 [1905.13534]. 2
- [30] L.-C. Qu, J. Chen and Y.-X. Liu, *Chaos and complexity for inverted harmonic oscillators*, *Phys. Rev. D* **105** (2022) 126015 [2111.07351]. 2
- [31] R.-Q. Yang, Y.-S. An, C. Niu, C.-Y. Zhang and K.-Y. Kim, *Principles and symmetries of complexity in quantum field theory*, *Eur. Phys. J. C* **79** (2019) 109 [1803.01797]. 2
- [32] P. Bueno, J.M. Magan and C.S. Shahbazi, *Complexity measures in QFT and constrained geometric actions*, *JHEP* **09** (2021) 200 [1908.03577]. 2
- [33] D.E. Parker, X. Cao, A. Avdoshkin, T. Scaffidi and E. Altman, *A Universal Operator Growth Hypothesis*, *Phys. Rev. X* **9** (2019) 041017 [1812.08657]. 3
- [34] V. Viswanath and G. Müller, *The Recursion Method: Application to Many-Body Dynamics*, Springer Berlin, Heidelberg 1994, . 3, 6
- [35] J.L.F. Barbón, E. Rabinovici, R. Shir and R. Sinha, *On The Evolution Of Operator Complexity Beyond Scrambling*, *JHEP* **10** (2019) 264 [1907.05393]. 3, 18
- [36] A. Dymarsky and A. Gorsky, *Quantum chaos as delocalization in Krylov space*, *Phys. Rev. B* **102** (2020) 085137 [1912.12227].
- [37] A. Dymarsky and M. Smolkin, *Krylov complexity in conformal field theory*, *Phys. Rev. D* **104** (2021) L081702 [2104.09514].
- [38] X. Zotos, *Operator growth in a quantum compass model on a Bethe lattice*, *Phys. Rev. B* **103** (2021) L201108.
- [39] D.J. Yates and A. Mitra, *Strong and almost strong modes of Floquet spin chains in Krylov subspaces*, *Phys. Rev. B* **104** (2021) 195121 [2105.13246].
- [40] P. Caputa, J.M. Magan and D. Patramanis, *Geometry of Krylov complexity*, *Phys. Rev. Res.* **4** (2022) 013041 [2109.03824].

- [41] J. Kim, J. Murugan, J. Olle and D. Rosa, *Operator delocalization in quantum networks*, *Phys. Rev. A* **105** (2022) L010201 [2109.05301].
- [42] P. Caputa and S. Datta, *Operator growth in 2d CFT*, *JHEP* **12** (2021) 188 [2110.10519].
- [43] D. Patramanis, *Probing the entanglement of operator growth*, *PTEP* **2022** (2022) 063A01 [2111.03424].
- [44] F.B. Trigueros and C.-J. Lin, *Krylov complexity of many-body localization: Operator localization in Krylov basis*, [2112.04722](#).
- [45] E. Rabinovici, A. Sánchez-Garrido, R. Shir and J. Sonner, *Krylov localization and suppression of complexity*, *JHEP* **03** (2022) 211 [2112.12128].
- [46] Z.-Y. Fan, *Universal relation for operator complexity*, *Phys. Rev. A* **105** (2022) 062210 [2202.07220].
- [47] R. Heveling, J. Wang and J. Gemmer, *Numerically Probing the Universal Operator Growth Hypothesis*, [2203.00533](#).
- [48] B. Bhattacharjee, X. Cao, P. Nandy and T. Pathak, *Krylov complexity in saddle-dominated scrambling*, *JHEP* **05** (2022) 174 [2203.03534].
- [49] K. Adhikari and S. Choudhury, *Cosmological Krylov Complexity*, [2203.14330](#).
- [50] W. Mück and Y. Yang, *Krylov complexity and orthogonal polynomials*, [2205.12815](#).
- [51] A. Banerjee, A. Bhattacharyya, P. Drashni and S. Pawar, *CFT to BMS: Complexity and OTOC*, [2205.15338](#).
- [52] N. Carabba, N. Hörnedal and A. del Campo, *Quantum speed limits on operator flows and correlation functions*, [2207.05769](#).
- [53] A. Bhattacharya, P. Nandy, P.P. Nath and H. Sahu, *Operator growth and Krylov construction in dissipative open quantum systems*, [2207.05347](#).
- [54] E. Rabinovici, A. Sánchez-Garrido, R. Shir and J. Sonner, *Krylov complexity from integrability to chaos*, *JHEP* **07** (2022) 151 [2207.07701].
- [55] C. Liu, H. Tang and H. Zhai, *Krylov Complexity in Open Quantum Systems*, [2207.13603](#). **3**
- [56] V. Balasubramanian, P. Caputa, J. Magan and Q. Wu, *Quantum chaos and the complexity of spread of states*, [2202.06957](#). **3, 6, 18, 23**
- [57] P. Caputa and S. Liu, *Quantum complexity and topological phases of matter*, [2205.05688](#). **3, 24, 25, 26**
- [58] P. Caputa, N. Gupta, S.S. Haque, S. Liu, J. Murugan and H.J.R. Van Zyl, *Spread Complexity and Topological Transitions in the Kitaev Chain*, [2208.06311](#). **3**
- [59] B. Bhattacharjee, S. Sur and P. Nandy, *Probing quantum scars and weak ergodicity-breaking through quantum complexity*, [2208.05503](#). **3**
- [60] P. Ribeiro, J. Vidal and R. Mosseri, *Exact spectrum of the lipkin-meshkov-glick model in the thermodynamic limit and finite-size corrections*, *Phys. Rev. E* **78** (2008) 021106. **3, 7**
- [61] P. Ribeiro, J. Vidal and R. Mosseri, *Thermodynamical limit of the lipkin-meshkov-glick model*, *Phys. Rev. Lett.* **99** (2007) 050402. **3, 7**
- [62] S. Campbell, *Criticality revealed through quench dynamics the Lipkin-Meshkov-Glick model*, *Phys. Rev. B* **94** (2016) 184403 [1608.05325]. **3**

- [63] K. Pal, K. Pal and T. Sarkar, *Nielsen complexity of coherent spin state operators*, [2106.11842](#). 3
- [64] H. Lipkin, N. Meshkov and A. Glick, *Validity of many-body approximation methods for a solvable model: (i). exact solutions and perturbation theory*, *Nuclear Physics* **62** (1965) 188. 6
- [65] S. Dusuel and J. Vidal, *Continuous unitary transformations and finite-size scaling exponents in the lipkin-meshkov-glick model*, *Phys. Rev. B* **71** (2005) 224420. 7
- [66] C.C. Gerry, *Correlated two-mode $su(1, 1)$ coherent states: nonclassical properties*, *J. Opt. Soc. Am. B* **8** (1991) 685. 9
- [67] M. Ban, *Decomposition formulas for $su(1, 1)$ and $su(2)$ lie algebras and their applications in quantum optics*, *J. Opt. Soc. Am. B* **10** (1993) 1347. 9, 25
- [68] M. Miyaji, S. Ryu, T. Takayanagi and X. Wen, *Boundary States as Holographic Duals of Trivial Spacetimes*, *JHEP* **05** (2015) 152 [[1412.6226](#)]. 24